Nanoscale Advances

ROYAL SOCIETY OF CHEMISTRY

REVIEW

View Article Online
View Journal | View Issue

Cite this: *Nanoscale Adv.*, 2020, **2**, 1380

Electronic structure engineering and biomedical applications of low energy-excited persistent luminescence nanoparticles

Qiaosong Lin, †[a] Zhihao Li,†[a] Chenhui Ji[b] and Quan Yuan *[ab]

Persistent luminescence nanoparticles (PLNPs) are new luminescent materials that can store the excitation energy quickly and persistently emit it after ceasing excitation sources. Due to the advantages of long-lasting luminescence without constant excitation, PLNPs have been widely used in biomedical applications. Visible light excitable PLNPs (VPLNPs) and near-infrared excitable PLNPs (NPLNPs) are two kinds of novel and promising PLNPs. Compared to conventional PLNPs, VPLNPs and NPLNPs have the characteristics of low tissue damage, deep tissue penetration, and high signal-to-noise ratio. With these special features, they have great potential in applications such as long-term tracing, deep-tissue bioimaging, and precise treatment. In this review, we introduce the common strategy of constructing VPLNPs and NPLNPs based on electronic structure engineering and the applications of VPLNPs and NPLNPs in biomedicine. This review article aims to offer valuable information about the progress and development direction of VPLNPs and NPLNPs, promoting more applications in biomedicine, materials science, energy engineering, and environmental technologies in the future.

Received 31st December 2019
Accepted 17th March 2020

DOI: 10.1039/c9na00817a

rsc.li/nanoscale-advances

1. Introduction

Persistent luminescence nanoparticles (PLNPs), also named as long afterglow nanoparticles, can quickly absorb the excitation energy and gradually emit luminescence for a long time after ceasing excitation sources.[1–4] The most important feature of PLNPs is the afterglow emission, which can last for minutes, hours, and even several years.[5–9] Owing to their long-lasting luminescence without constant illumination, PLNPs are usually exploited as lighting components for safety signage,[10] decoration,[11,12] and displays.[13] Furthermore, in biological detection[14–16] and imaging,[17–20] the advantage of long life-time emission also ensures that autofluorescence interference can be eliminated successfully.[21,22] Benefiting from this unique feature, PLNPs have already received much attention in bio-analysis in recent decades.[23,24] However, the excitation band of conventional PLNPs is usually located in the ultraviolet (UV) region.[25,26] The high energy UV ray invariably causes strong

[a]*Key Laboratory of Analytical Chemistry for Biology and Medicine (Ministry of Education), College of Chemistry and Molecular Sciences, Wuhan University, Wuhan 430072, China. E-mail: yuanquan@whu.edu.cn*

[b]*Institute of Chemical Biology and Nanomedicine, State Key Laboratory of Chemo/Biosensing and Chemometrics, College of Chemistry and Chemical Engineering, Hunan University, Changsha 410082, China*

† These authors contribute equally to this work.

Qiaosong Lin is a BS candidate in Prof. Quan Yuan's research group at College of Chemistry and Molecular Sciences, Wuhan University. His current research interests include the luminescence mechanism and biological applications of persistent luminescence nanomaterials.

Zhihao Li received his BS degree from the College of Chemistry and Molecular Sciences, Wuhan University, in 2016. Currently, He is a PhD candidate in Prof. Quan Yuan's research group at Wuhan University. His current research interests include the design and applications of luminescence nanoparticles.

tissue damage and has low tissue penetration.[27] These drawbacks totally restrict their further utilization in biological areas, especially in long-term tracing, deep-tissue bioimaging, and precise therapy. To be specific, UV excitation of PLNPs usually causes unnecessary tissue damage to the body and unnecessarily increases pain in patients. Besides, PLNPs should be excited with UV light, which also results in low excitation efficiency during *in vivo* bioimaging due to the low tissue penetration of UV light.[17,28] Therefore, it is particularly significant to propose new regulation strategies to extend the excitation bands of PLNPs from the UV region to the longer wavelength region such as visible light region and near infrared (NIR) region.

Generally, the range of the excitation band of PLNPs depends on the energy difference between the ground state and excited state of electrons.[3,29,30] Tuning the electron structures is the most effective strategy to modulate the excitation band. In this regard, electronic structure engineering strategies such as doping[31,32] and etching[33,34] have already been used by researchers to extend the excitation bands of PLNPs to the visible light region and the NIR region. In 2011, Pan *et al.* successfully extended the excitation band to the visible light region by doping Cr^{3+} ions into PLNPs.[12] Also, in 2014, Pan's group extended the excitation band to the NIR region by incorporating the up-converting ion pair Yb^{3+}/Er^{3+}.[35] The development of visible light excitable PLNPs (VPLNPs) and NIR excitable PLNPs (NPLNPs) is important for PLNPs in the promotion of further biomedical applications. As for VPLNPs, the excitation by visible light has lower tissue damage than that by UV energy.[36–38] In this condition, VPLNPs can be re-activated multiple times *in vivo* without additional tissue damage so that it is more suitable for long-term *in vivo* tracing and bioimaging.[39] Besides, for NPLNPs, the excitation NIR light has strong tissue penetration.[28] Therefore, NPLNPs can be re-activated in deep tissues *in situ* and have advantages in deep-tissue bioimaging and tracing.[40] In short, VPLNPs and NPLNPs have great potential to play important roles in establishing *in situ* life science imaging systems and precision diagnosis and treatment platforms in the future; to summarize, the construction strategies and applications of VPLNPs and NPLNPs will have positive effects on further development.

In this review article, we provide a summary of the current developments in VPLNPs and NPLNPs with their recent progress in biomedical applications. Firstly, a brief description of persistent luminescence mechanism is presented. Then, we introduce the strategy for extending the excitation band to the visible light region based on the Stokes mechanism. After discussing the strategy, the application of VPLNPs in the biomedical field will be presented, especially in biodetection, bioimaging, and imaging guided treatment. Following the introduction of VPLNPs, the strategy of extending the excitation band to the NIR region is discussed with the applications of NPLNPs in disease diagnosis and precise treatment. At the end of this review, an evaluation of the current challenges and the outlook for the development of VPLNPs and NPLNPs are also put forward. The aim of this review is to provide valuable information about the progress and development direction of VPLNPs and NPLNPs, and to make positive effects on their improvement of synthesis and further applications.

2. Brief description of persistent luminescence

In order to effectively control the luminescent properties of PLNPs *via* electronic structure engineering, understanding the mechanism of persistent luminescence is very important. In this section, we will introduce the brief mechanism of persistent luminescence.

The schematic diagram of persistent luminescence is shown in Fig. 1.[41] For PLNPs, there are two main elements acting as important parts in persistent luminescence: emitters and traps.[29,42] Emitters usually consist of transition metal ions or lanthanide ions doped in a host material, which forms the ground state energy level and a series of excited state energy levels. The distribution of emitters is sporadic, so the ground state and excited state formed by the emitter will not expand to the whole crystal. Traps in PLNPs can be formed by co-dopants or intrinsic crystal defects, and the energy of the traps is usually a few electronic volts lower than the conduction band of the

Chenhui Ji received her BS from the School of Chemistry and Chemical Engineering, Inner Mongolia University of Science and Technology in 2015. She is pursuing her PhD degree at the College of Chemistry and Chemical Engineering, Hunan University, and is currently working in Professor Quan Yuan's research group. Her research interests include the development of functional nanomaterials for biosensing and therapy.

Professor Quan Yuan obtained her PhD degree from the College of Chemistry and Molecular Engineering, Peking University, in 2009. Later, She continued her postdoctoral research at the University of Florida. In 2012, She joined the College of Chemistry and Molecular Sciences, Wuhan University, as a full professor. Her research focuses on the controlled synthesis of functional nanomaterials and exploring their biomedical applications.

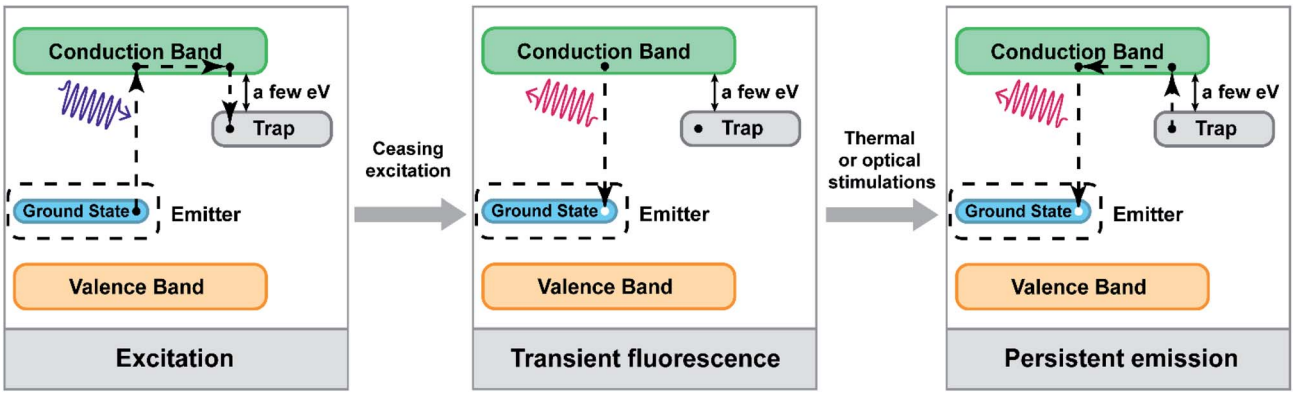

Fig. 1 Schematic diagram of persistent luminescence (adapted with permission from ref. 41. Copyright 2019 Elsevier).

host material. Electrons in the ground state of the emitters absorb photons and are excited to a higher energy level or the conduction band. Then, some electrons in the conduction band will be caught by electron traps and this process stores the energy in the traps in the form of electrons. After stopping the excitation light, with thermal motion or external stimulation, these electrons will be slowly released to the conduction band and return to the ground state of the emitters, which generates long persistent luminescence. The lifetime of afterglow depends on the number of electrons caught by the traps and the persistent luminescence intensity depends on the rate of return of electrons in the traps to the ground state of the emitter.

In this process, the distribution of energy levels in the emitters and the depth of traps play important roles in persistent luminescence and will affect the wavelength range of the excitation and emission bands. If the ground state of the emitter is closer to the conduction band of the host material, the necessary energy of the photons is lower and the wavelength of the excitation band shifts to the long wavelength region. Besides, if there are some other excited energy states of the emitters between the conduction band and the ground state, their energy eigenvalues are close to the energy eigenvalues of the traps; electrons can also be filled into the traps with quantum tunnelling effect instead of passing through the conduction band. Moreover, doping up-conversion ions as emitters, which can utilize the up-conversion process to fill electrons into the traps, is also a strategy to change the excitation wavelength. Therefore, it is possible to change these conditions of PLNPs *via* electronic structure engineering and to construct VPLNPs and NPLNPs.

3. Electronic structure engineering of VPLNPs and their applications

Owing to the good biocompatibility, low energy consumption, and ease of use, visible light has been regarded as one of the ideal excitation light sources.[12] VPLNPs can be excited by visible light so that they have several great advantages during long-term biological detection, biological imaging, and imaging-guided therapy, such as elimination of autofluorescence and reduction of tissue damage.[11] During long-term bioimaging, VPLNPs can be re-excited multiple times *in vivo* with visible light, which will not generate additional tissue damage.[37,43,44] This makes VPLNPs potential candidates for long-term *in vivo* tracking.[45,46] The development of VPLNPs will significantly promote the building of precision diagnosis and treatment platforms, and bring positive impacts in life sciences, materials science, energy engineering, and environmental testing in the future.

3.1. Tuning strategies based on Stokes mechanism

The luminescence mechanism of most PLNPs follows the Stokes mechanism. The process is shown in Fig. 2a; the electrons are excited from the ground state to the excited state by absorbing only one photon for once. Then, the electrons in the excited state undergo a series of non-radiative transition processes such as vibrational relaxation, intersystem crossing, and internal conversion. After ceasing the excitation light, these electrons return to the ground state from the lowest vibrational energy level of the excited state and emit a photon. In this condition, the emission wavelength is usually larger than the excitation wavelength.[47–49] Therefore, the effective strategy for extending the PLNPs excitation band to the visible light region is based on its Stokes luminescence mechanism and the key to this strategy is to construct a reasonable excited state.

In 2012, Pan and his co-workers pointed out a strategy to extend the excitation band to over 600 nm.[12] The VPLNP was synthesized by doping Cr^{3+} into zinc gallogermanates (ZGGO) (Fig. 2b). After doping the Cr^{3+} ion, generation of $^4A_2$, $^4T_2(t^2e)$, $^4T_1(t^2e)$ and $^4T_1(te^2)$ energy levels between the valence band and conduction band occurs (Fig. 2b). Among them, $^4A_2$ is the ground state of Cr^{3+} and the difference in the energy between $^4A_2$ and $^4T_1(t^2e)$ is approximately in the visible light wavelength range. Through the detection of the excitation spectrum, the authors monitored a very board excitation band from 300 nm to 650 nm, corresponding to three inner transitions of Cr^{3+}, including $^4A_2 \rightarrow {}^4T_1(te^2)$, $^4A_2 \rightarrow {}^4T_1(t^2e)$, and $^4A_2 \rightarrow {}^4T_2(t^2e)$. The transition $^4A_2 \rightarrow {}^4T_2(t^2e)$ will originate the 568 nm excitation peak. Besides, according to the authors, there is a linear dependence between the reciprocal persistent luminescence

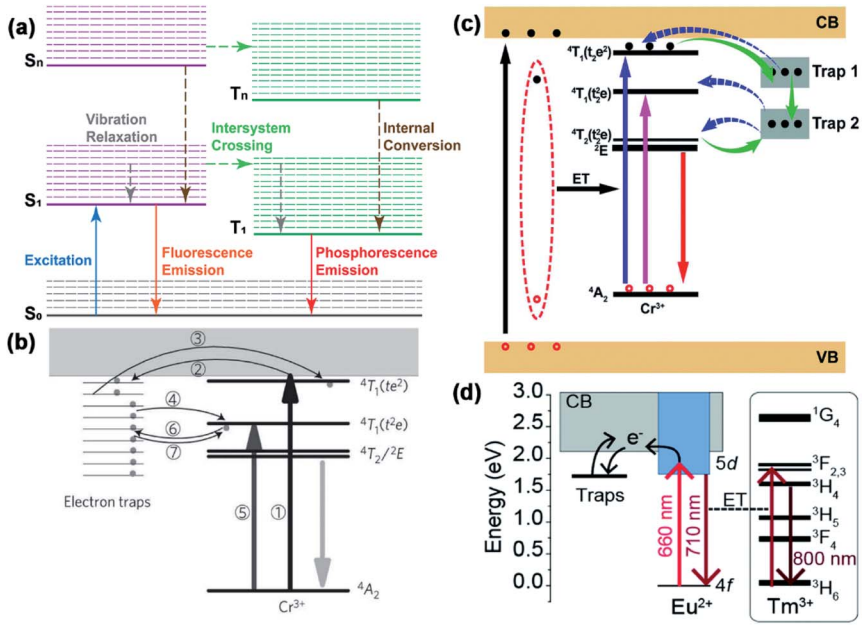

Fig. 2 (a) Schematic diagram of Stokes mechanism. S_0 is the ground state, S_1 is the first excited singlet state, and T_1 is the first excited triplet state. The solid lines represent the electronic energy levels and the dashed lines represent the vibrational energy levels. Solid arrows indicate radiative transitions and dotted arrows indicate non-radiative transitions. (b) Scheme of electronic structure engineering by Cr^{3+} doping (adapted with permission from ref. 12. Copyright 2011 Nature). (c) Scheme of electronic structure engineering by the generation of deep traps (adapted with permission from ref. 50. Copyright 2017 Royal Society of Chemistry). (d) Scheme of electronic structure engineering by Eu^{2+} doping (adapted with permission from ref. 52. Copyright 2019 Royal Society of Chemistry).

intensity (I^{-1}) and time (t), which represents the quantum tunnelling effect during the process. Considering that the energy of $^4T_1(t^2e)$ is close to the energy of the traps, electrons in $^4T_2(t^2e)$ can be filled in the traps with quantum tunnelling effect and be released back by reverse tunnelling recombination but should not pass through the conduction band. The kinetic rate of quantum tunnelling effect and reverse tunnelling recombination is slow so that it will cause persistent luminescence. In this condition, the excitation band of PLNP is successfully broadened to the visible light region according to Stokes mechanism. Therefore, through construction of $^4A_2 \rightarrow {}^4T_2(t^2e)$ excitation by doping Cr^{3+}, the excitation band of PLNPs can be effectively extended to the visible light region.

After Pan's work, Zheng and Chen *et al.* used $ZnGa_2O_4$ as a host material, which is different from Pan's ZGGO.[50] According to the calculation by Chen's equation:[51]

$$E_t = n_0\left(\frac{k_B T_m{}^2}{\omega}\right) - 2k_B T_m$$

$$n_0 = \frac{\omega I_m}{\beta\left[2.52 + 10.2\left(\frac{\delta}{\omega} - 0.42\right)\right]}$$

In this equation, ω stands for the full width at half maximum of the thermoluminescence band, δ is the high-temperature fitting factor, T_m and I_m are the temperature and intensity, β represents the rate of heat. They put forward that there are shallow traps (0.49 eV) and deep traps (0.91 eV) in $ZnGa_2O_4$, and these traps are usually generated with inherent lattice defects of $ZnGa_2O_4$. Deep traps can also capture electrons from $^4T_2(t^2e)$ of Cr^{3+} through quantum tunnelling and release back *via* reverse tunnelling recombination. This process only needs to excite the electrons from $^4A_2$ to $^4T_2(t^2e)$ whose excitation energy is in the visible light region and can also cause persistent luminescence (Fig. 2c).

In addition to Cr^{3+} doping, Ueda *et al.* put forward a new strategy of co-doping Eu^{2+} and Tm^{3+} into $Ba[Mg_2Al_2]N_4$.[52] With the doping of Eu^{2+}, two separate energy levels between the valence band and the conduction band of $Ba[Mg_2Al_2]N_4$ will be generated. As a feature of rare earth elements,[53] the gap between 4f and 5d is not so wide and the electrons in 4f can be excited to 5d *via* long wavelength visible light. Besides, the excitation state 5d is close to the conduction band of $Ba[Mg_2Al_2]N_4$ and the electrons in 5d can be caught by traps through the conduction band (Fig. 2d). According to the authors' characterization of the excitation spectrum, this VPLNP has a wide excitation band in the visible light region from 400 nm to 650 nm and these excitation bands are attributed to the host-to-band absorption and Eu^{2+} transitions from 4f to 5d. Plus, when the electrons are released from the traps and return to the 4d energy level, the emitted energy can be transmitted to Tm^{3+} without radiation. Tm^{3+} can make the emission wavelength redshift to the NIR region by the excitation–relaxation–radiation process. With the strategy of Ueda *et al.*, the excitation band is successfully extended to the visible light region, even to the red-light region.

In short, doping Cr^{3+} ions, which utilizes the quantum tunnelling effect of electrons between the excited states of Cr^{3+} and electron traps to achieve visible light excitation, is one of the most effective methods at present. Except for this method, similar purposes can also be achieved by regulating the depth of electron traps through defects in the host materials or by doping of other ions. In this regard, electronic structural engineering has already played major roles in extending the excitation band of PLNPs into the visible light region. However, the strategies are still insufficient and the efficiency of excitation by visible light is not high enough. Therefore, developing more strategies and improving the efficiency of excitation by visible light are bottlenecks that need to be overcome in the future development of VPLNPs.

3.2. Application of VPLNPs in biomedicine

While researching the strategies of constructing VPLNPs, scientists have begun to focus on the applications of VPLNPs in recent years. More and more VPLNPs are applied in many biomedical areas, especially in biodetection, bioimaging for diagnosis, and precise treatment.[54] In this subsection, we will introduce the recent progress in the applications of VPLNPs in biodetection, bioimaging, and guided disease treatment.

3.2.1. Biodetection. Biodetection is one of the most essential technologies in bioanalysis,[55] including the detection of various biological indicators such as proteins,[56–58] nucleic acids,[2,59] biological small molecules,[15,60,61] and physiological parameters.[23,62] These technologies have already played important roles in disease diagnosis,[18–20] water quality monitoring,[63] food and drug safety survey,[6] and criminal investigations.[65,66] Among various biodetection technologies, fluorophotometry provides a convenient,[67,68] real-time,[69–72] and non-invasive[73–75] method for detecting analyte contents, and is one of the most promising quantitative detection technologies.[76]

Up to now, scientists have already developed several fluorescent probes for fluorophotometry, all of which play crucial roles in selective biodetection.[71–75,77–79] However, in complex biological environments, these probes are typically affected by strong background fluorescence generated by biological substrates.[80] Due to the need of sustained excitation, it will significantly reduce the sensitivity and limit of detection. Usually, the fluorescence lifetime of biological substrates is only a few nanoseconds.[41] In this condition, VPLNPs can effectively reduce the background fluorescence of the substrates because the fluorescence generation by substrates will be eliminated after ceasing excitation and VPLNPs still have longer afterglow. Therefore, the use of VPLNPs as probes for biological detection can improve the sensitivity and limit of detection. In this regard, VPLNPs are expected to be applied as imaging probes for disease diagnosis and biological process research.

In 2017, Zheng and Chen *et al.* used biotinylated $ZnGa_2O_4$:Cr^{3+} as a sensitive and specific luminescent nanoprobe for the detection of avidin in heterogeneous bioassays.[50] The author combined biotin with PLNPs by electrostatic attraction or chelation of Zn^{2+}/Ga^{3+}. Due to the strong affinity of biotin–avidin, biotinylated VPLNPs probes can specifically target avidin or avidin-bridged biotinylated antibodies (Fig. 3a). The authors quantified the concentration of avidin by measuring the afterglow signal of biotinylated PLNP and obtained a good quantitative curve, which had excellent linear response in the low concentration range (Fig. 3b). Furthermore, since $ZnGa_2O_4$:Cr^{3+} can be effectively excited by visible light, the background fluorescence interference is greatly reduced (Fig. 3c). In this regard, they obtained lower detection limits and good sensitivity, which reveals the great potential in ultrasensitive biodetection.

In 2018, Wang and his co-authors developed a kind of unique VPLNP probe for detecting food-borne aflatoxin *in vivo*.[64] Wang *et al.* constructed the VPLNP by co-doping Cr^{3+}, Yb^{3+}, and Er^{3+} into ZGGO. The aptamer was modified on the surface of VPLNP probes and combined with ssDNA-modified CuS nanoparticles. At first, CuS can quench the fluorescence of VPLNP probe. After the concentration of aflatoxin increases, aflatoxin B1 will compete with ssDNA-modified CuS nanoparticles and substitute them to combine with the aptamer, which will recover the fluorescence of the VPLNP probe. With co-doping of Cr^{3+}, Yb^{3+}, and Er^{3+}, these probes can be excited by red LED light (650 ± 10 nm) *in vivo* and have long afterglow life. Thus, these probes have several advantages such as high signal-to-noise ratio, wide linear range (0.1–2.4 μM), and lower detection limit (0.03 μM). In this regard, these probes exhibit great potential in food safety testing and are expected to be developed into an *in situ* nano detection platform for monitoring food safety.

In conclusion, as VPLNPs can effectively decrease the background fluorescence of the substrate, VPLNPs have high signal-to-noise ratio in biodetection. In this regard, VPLNPs are ideal candidates for *in situ* detection in complex biological matrices and it is expected that VPLNPs will have better performance in highly selective and sensitive nano detection platforms.

3.2.2. Bioimaging. Bioimaging is a vital method to investigate the physiological and pathological mechanisms and

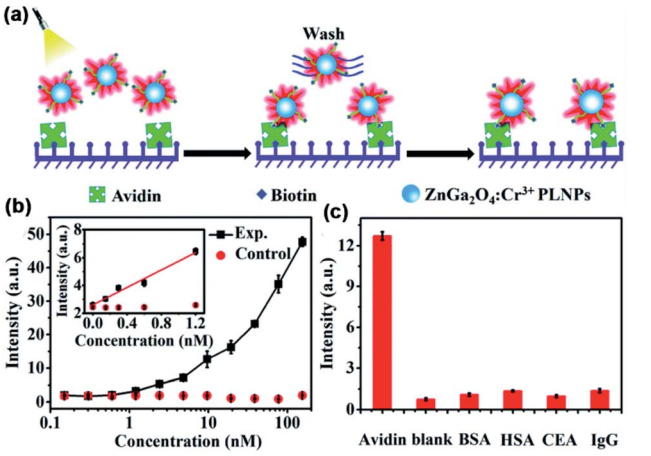

Fig. 3 (a) Schematic diagram of heterogeneous $ZnGa_2O_4$:Cr^{3+} VPLNPs assay of avidin. (b) Quantitative standard curve for the biodetection by utilizing $ZnGa_2O_4$:Cr^{3+} VPLNPs. (c) Specificity of the assay utilizing non-cognate proteins as the control (adapted with permission from ref. 50. Copyright 2017 Royal Society of Chemistry).

provides significant information for disease diagnosis and treatment.[69,81] Among various imaging techniques, fluorescence bioimaging provides a non-invasive and visual approach to monitor the biological processes[82,83] and has been regarded as one of the most powerful imaging tools.[73–75] For bioimaging, numerous fluorescent probes based on organic dyes,[21,43] quantum dots,[43] fluorescent proteins, and metal complexes have been developed and play significant roles in labelling the targets. However, these probes should be excited during the whole imaging process. At the same time, the light source can also excite other matrix molecules in the tissues, leading to intense autofluorescence.[80] Such intense autofluorescence would strongly affect the fluorescent signal of the targets of interest and hamper the improvement in imaging sensitivity and accuracy.

Given that the fluorescent lifetime of proteins and small molecules is below nanoseconds, PLNPs are ideal alternatives to these traditional fluorescent probes for bioimaging because the lifetime of PLNPs can reach several minutes and hours.[5,6] VPLNPs probes can be excited by visible light effectively and multiple times in the body. During long-term biological imaging, it can reduce the tissue damage generated by the excitation process, which can effectively reduce the pain of patients.[43] In this regard, VPLNPs hold great promise for the construction of imaging probes for disease diagnosis and investigation of biological processes.

According to what we mentioned in Section 3.1, utilizing Cr^{3+} doping with its transition $^4A_2 \rightarrow {}^4T_2(t^2e)$ is an effective method to extend the excitation band of PLNPs to the visible light region. In 2015, Prof. Han and his group utilized mesoporous $SiO_2/ZnGa_2O_4:Cr^{3+}$ persistent luminescence nanocomposites as imaging probes.[36] According to the authors, the novel persistent luminescence nanocomposites can be repeatedly charged *in vivo* by a white LED or even red light (620 nm). This property demonstrates that these nanocomposites are suitable for rechargeable long-term bioimaging. In addition to Han's work, our group also made progress in the bioimaging application of VPLNPs recently.[39] We synthesized ZGGO nanoparticles $Zn_{1+x}Ga_{2-2x}Ge_xO_4:Cr^{3+}$ (x = 0–0.5) and assembled ZGGO:Cr^{3+}-aptamer nanocomposites to target cancer cells. We demonstrated that with Cr^{3+} doping, ZGGO can be activated *in* vivo by commercialized orange LED (550 nm) effectively (Fig. 4a). Besides, we also noticed that the size and persistent luminescence decay time of the nanoparticles can be easily controlled by changing the concentration of Ge. Compared to the cyanine-derivative dye and Ag_2Se, autofluorescence of ZGGO:Cr^{3+}-aptamer nanocomposites is significantly decreased (Fig. 4b). Besides, the nanocomposites also exhibit high affinity for the tumour and good biocompatibility. Under the circumstances, the nanocomposites are ideal materials for autofluorescence-free tumour targeted bioimaging *in vivo* and cancer diagnosis.

In addition to Cr^{3+} doping, scientists have also used some VPLNPs doping by other ions in bioimaging. In 2019, Ueda *et al.* doped Eu^{2+} and Tm^{3+} into $Ba[Mg_2Al_2N_4]$.[52] According to the authors, they monitored that this VPLNP has a wide excitation band in the visible light region from 400 nm to 650 nm. In addition, due to the doping of Tm^{3+}, the VPLNP also has near-infrared emission bands, which can effectively solve the problem of biological tissue penetration. The authors confirmed that the VPLNP can indeed be excited by a red LED. Besides, the emitted light is in the near-infrared light region, which shows that this the emission light of VPLNP has good tissue penetration. Due to the characteristics of long afterglow, the VPLNP has a high signal-to-noise ratio and low background fluorescence, and the stability and repeatability of continuous light emission are reliable. Therefore, with the properties of long afterglow and red LED excitation, this persistent phosphor has the potential to be used as a persistent luminescent probe for *in vivo* long-term imaging.

Hence, because the visible excitation light has better compatibility with living organisms, using visible light as the excitation source will not cause the same serious tissue damage as UV excitation. In this way, VPLNPs exhibit great potential in biological imaging, especially long-term bioimaging and tracking. In the future, VPLNPs will play important roles in building platforms for imaging and disease diagnosis.

3.2.3. Guiding for disease treatment. With the development of medicine and the increase in the proportion of patients with tumour diseases, building a precise treatment platform will become a trend in future biomedical fields.[84,85] Especially for the treatment of malignant tumours, traditional chemotherapy and radiotherapy schemes have brought great pain to patients and have caused serious damage to the patients' bodies. In order to solve these issues, the development of imaging-induced precise therapies is of great significance to overcome malignant tumour diseases.[86,87] VPLNPs can be excited by visible light, which avoids extra light damage caused by *in vivo* excitation and is one of the important fluorescent probes for imaging-guided precise treatment.[88,89] Without background fluorescence, VPLNPs has high signal-to-noise ratio, long luminous time, and have received widespread attention from scientists in recent years.

Accurate drug delivery is one of the important strategies for accurate treatment.[86,87,90–92] Through the imaging and tracking of drug carriers, medical staff can monitor the distribution of drugs can in real time and determine the plan of treatment for the next step. In 2015, Zhang *et al.* developed multifunction VPLNPs for drug delivery and targeted tumour imaging.[46] The authors prepared porous VPLNP probes $Zn_{1.1}Ga_{1.8}Ge_{0.1}O_4:Cr^{3+},Eu^{3+}@SiO_2$ and modified the surface with folic acid. These probes can not only be loaded with a large amount of doxorubicin hydrochloride but are also able to target tumours with high sensitivity (Fig. 4c). Also, these modified nanoprobes can be re-excited *in vivo* by red LED lights, which enables the nanoprobes to be applied for long-term background-free cell tracking and monitoring *in vivo*. Except for Zhang's work, recently, Fu and co-authors constructed a new type of tumour-targeting drug platform.[45] They used $ZnGa_2O_4:Cr^{3+},Sn^{4+}$ as the fluorescence part and covered mesoporous silica at the surface of $ZnGa_2O_4:Cr^{3+},Sn^{4+}$ to load the drug. Except for that, authors also modified hyaluronic acid on the outer surface of mesoporous silica as the targeting part of these probes. Due to the transition $^4A_2 \rightarrow {}^4T_2(t^2e)$ in Cr^{3+}, these probes can be re-excited by visible light (550 nm) *in vivo*, which exhibits that these probes

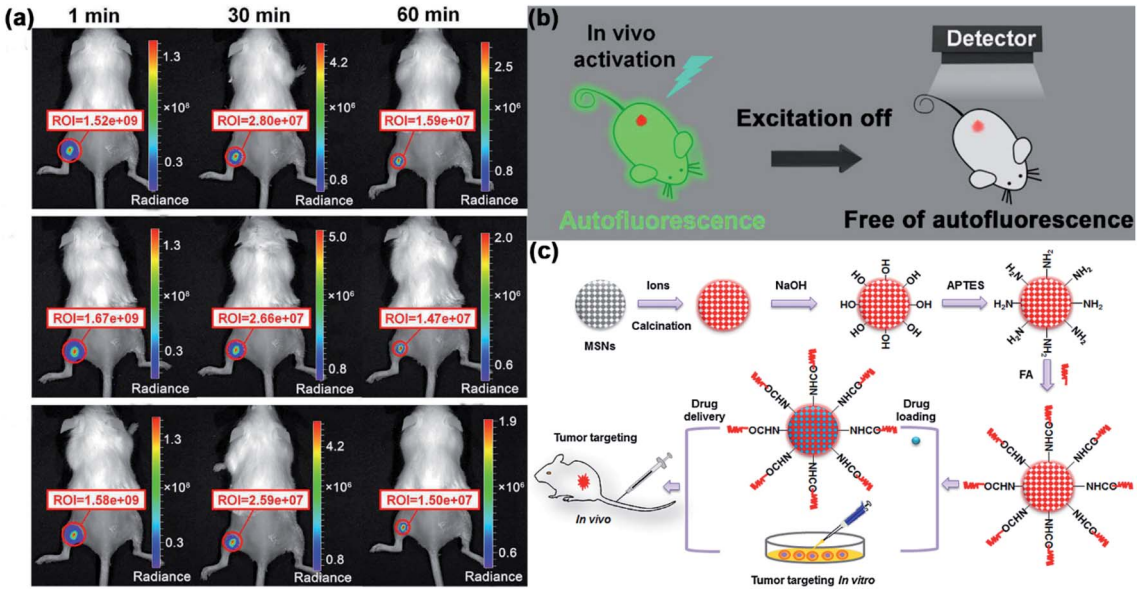

Fig. 4 (a) Images of Cr^{3+}-aptamer probes in *in vivo* bioimaging after the first (top), second (middle), and third (bottom) excitations by orange LEDs. (b) Schematic diagram of eliminating autofluorescence interference in bioimaging by using Cr^{3+}-aptamer probes (adapted with permission from ref. 39. Copyright 2017 American Chemical Society). (c) Schematic diagram for the synthesis, surface modification, and application of VPLNPs in bioimaging and tracking of drug delivery (adapted with permission from ref. 46. Copyright 2015 Elsevier).

can be applied in reproducible and highly sensitive bioimaging. According to the authors, they have successfully delivered the non-fluorescent chemotherapeutic drug (paclitaxel) to human breast adenocarcinoma cells and monitored the distribution of the nanoplatforms by luminescence imaging. Therefore, it is reasonable to believe that this nanoplatform can become a promising tool for bioimaging guided drug delivery and can effectively reduce the side effects.

In addition to tracking drug carriers, VPLNPs can also be effectively used in photodynamic therapy. Photodynamic therapy is an effective non-invasive treatment method.[93–97] It generates reactive oxygen species (ROS) through photodynamic reaction and uses ROS to kill the tumour cells.[27,98–100] In 2017, Huang and Chen *et al.* used $ZnGa_{1.996}O_4{:}Cr_{0.004}{}^{3+}$ as a photodynamic excitation light source.[80] This VPLNP can be excited by white LED *in vivo* and the NIR emission can activate the photochlor 2-(1-hexyloxyethyl)-2-devinyl pyropheophorbide-α (HPPH). HPPH, with the activation of VPLNP, will release ROS (Fig. 5). According to the authors, the growth of the tumour was effectively inhibited. Tumours after LED irradiation shrank significantly within one week and showed massive tissue apoptosis and necrosis. This is mainly due to ROS mediated damage. In this condition, it proves that repeatable photodynamic therapy based on VPLNP as the light source achieves the best therapeutic effect. Thus, VPLNPs also have wide application potential photodynamic therapy.

Moreover, bioimaging guided surgery has also gradually attracted the attention of scientists. Surgical treatment is more direct and more thorough, which is the main method of treating tumours at present. Imaging-guided surgery can effectively improve the accuracy and safety of surgery and reduce excessive resection of the non-lesioned tissue.[101] In 2019, Ding *et al.* developed an organic VPLNP as a probe to guide cancer surgery with precise imaging.[43] This organic VPLNP can be effectively excited by visible light and generates NIR emission, which can provide nearly 100 times higher ratio of tumour to liver than that by traditional fluorescence imaging (Fig. 6). Ultra-high tumour-to-liver signal ratio and low afterglow background noise make for excellent performance in accurate imaging-guided cancer surgery. In addition, it has a very long afterglow life (more than 6 hours), which is also more favourable for long-term tumour surgery. In this regard, organic VPLNP has great potential in imaging-guided surgery.

In short, due to the good biocompatibility of visible light, VPLNPs can effectively reduce tissue damage during the imaging process as probes for imaging-guided therapy. In addition, with the long afterglow characteristics of VPLNPs, they have an extremely high signal-to-noise ratio, which can provide clear imaging for precise treatment. Consequently, VPLNPs will play significant roles in the development of imaging-guided therapy in the future.

4. Electronic structure engineering of NPLNPs and their applications

In addition to the long-term and *in situ* diagnosis and treatment platform, deep tissue imaging technology is also an important research trend and direction of modern medical technology. NIR is in the biological transparent window and has good tissue penetrability, which has attracted much attention. By extending the traditional PLNPs excitation band to the NIR region, PLNPs can be excited effectively in the deep tissue by NIR and applied in deep-tissue bioimaging.[28,35] Besides, with small background fluorescence of NPLNPs, they can also improve the signal-to-

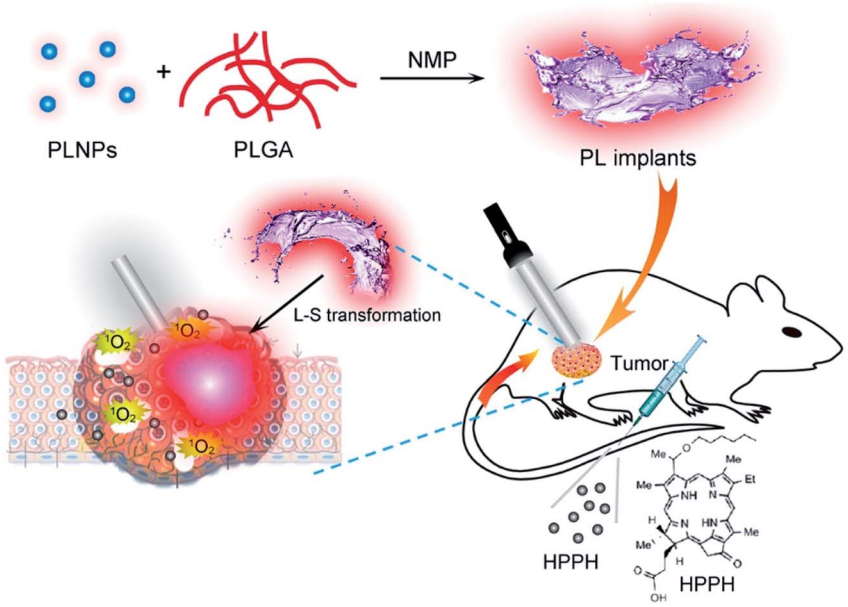

Fig. 5 Schematic illustration of the construction of VPLNPs for photodynamic therapy (adapted with permission from ref. 80. Copyright 2017 American Chemical Society).

noise ratio. In this regard, NPLNPs can play important roles in establishing deep-tissue diagnosis and treatment platforms. In this section, we will introduce the main strategies for extending the excitation band of PLNPs to the NIR range and its application in the field of biomedicine.

4.1. Tuning strategies based on anti-Stokes mechanism

Under the condition of Stokes mechanism, NIR cannot bring enough photoexcitation energy to enable PLNPs to be effectively activated. Therefore, we need to design a new electronic structure engineering strategy so that the excitation band of PLNPs can be extended to the NIR region. The most common one is to use the anti-Stokes mechanism to achieve the excitation of PLNPs.[102,103] In this section, we will discuss the strategies based on anti-Stokes mechanism for NPLNPs.

According to Pan *et al.*, the strategy for expand the excitation band to NIR region includes the construction of up-conversion luminescence process into a persistent luminescence process.[35] Up-converted luminescence consists of the following steps: (1) electron in the ground state absorbs one photon and transfers

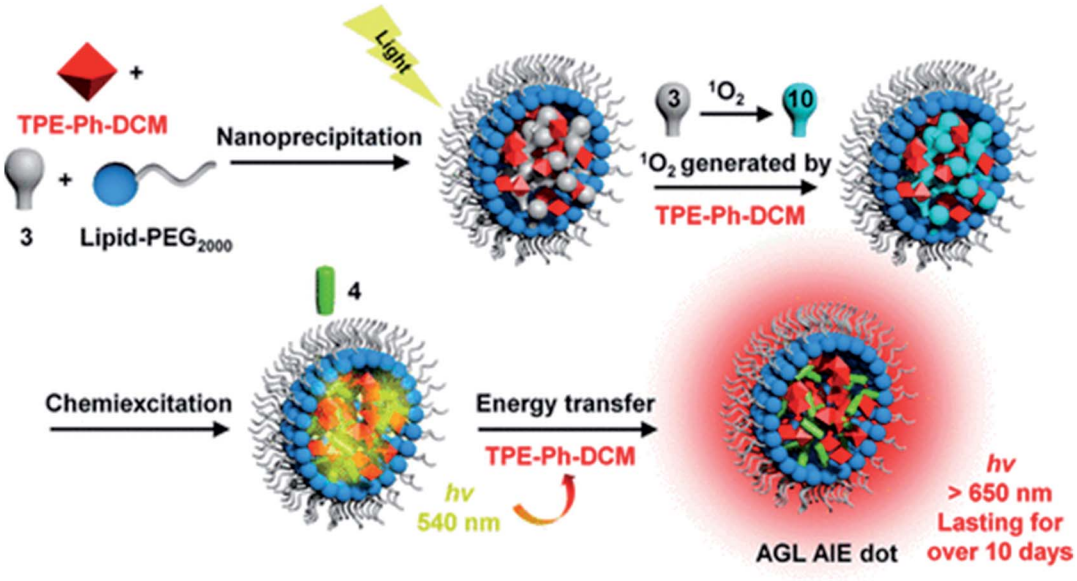

Fig. 6 Schematic diagram of the construction of organic long afterglow probes for imaging-guided surgery (adapted with permission from ref. 43. Copyright 2019 American Chemical Society).

to the metastable state. (2) Electrons in the metastable state transfer to a higher state by non-radiative relaxation or absorption of another photon. (3) When the number of electrons in the higher state is enough to form a population inversion, the electrons in higher state will return to the ground state and achieve high frequency emission. For NPLNPs, the electrons in the metastable state can transfer to the delocalized state by non-radiative relaxation. Some electrons in the delocalized state will return to the ground state and lead to transient fluorescence, and other electrons will be caught by electron traps (Fig. 7a). After ceasing the excitation light, with the thermal motion or external stimulation, the electrons in the traps will be released to the delocalized state again slowly. This part of the electrons will finally return to the ground state and lead to persistent luminescence. Therefore, constructing a suitable up-conversion system to promote PLNPs excitation is an important way to construct NPLNPs. The common method to convert an up-conversion system into persistent luminescence is to co-dope with some up-conversion ions as emitters or form some complexes of upconverted particles with PLNPs as the emitters.

In 2017, Zeng and Hao *et al.* provided a method for constructing NPLNPs with anti-Stokes mechanism. They doped Yb^{3+} and Er^{3+} into ZGGO:Cr^{3+}, and these two up-conversion ions can cooperate with Cr^{3+} as an anti-Stokes emitter.[40] For this NPLNPs, Yb^{3+} ion will generate $^2F_{7/2}$ and $^2F_{5/2}$ energy levels, and Er^{3+} will generate a series of energy levels (from low energy to high energy: $^4I_{15/2}$, $^4I_{13/2}$, $^4I_{11/2}$, $^4I_{9/2}$, $^4F_{9/2}$, $^4S_{3/2}$, $^2H_{11/2}$, and $^4F_{7/2}$) between the conduction band and valence band of the host material. The electrons in $^2F_{7/2}$ of Yb^{3+} can be excited to $^2F_{5/2}$ by NIR and can then be transferred to $^4F_{7/2}$ of Er^{3+} through one step or multi-step non-radiative relaxation. Except for the electrons in Yb^{3+}, electrons in $^4I_{15/2}$ of Er^{3+} can also be excited to $^4I_{11/2}$ *via* NIR and can then be transferred to $^4F_{7/2}$ by non-radiative relaxation. Electrons in $^4F_{7/2}$ can relax to $^2H_{11/2}$, $^4S_{3/2}$, and $^4F_{9/2}$, then electrons in $^2H_{11/2}$ and $^4S_{3/2}$ can be transferred to $^4T_2$ of Cr^{3+} *via* relaxation and can be caught by traps (Fig. 7b). The entire processes form the part of filling electrons into the traps through the anti-Stokes mechanism, which shows that NPLNPs can be excited *via* NIR. After ceasing the excitation, the traps in ZGGO will slowly release the electrons to $^4T_2$ of Cr^{3+} and turn back to $^4A_2$, causing persistent luminescence. Thus, it is practical to extend the excitation band of PLNPs to the NIR region by co-doping Yb^{3+}, Er^{3+}, and Cr^{3+} into ZGGO.

Apart from Zeng and Hao's work, Feng and Li *et al.* also put forward another method to construct NPLNPs.[104] According to Feng and the co-authors, they synthesized a composite structure that can also carry out such similar electron transfer processes (Fig. 7c). For this composite structure, PLNPs ZGGO:Cr^{3+} were covered by up-conversion nanoparticles β-$NaYbF_4$:Tm^{3+}@$NaYF_4$. After the electrons in $^2F_{7/2}$ of Yb^{3+} absorb NIR and are excited to $^2F_{5/2}$, the electrons in $^2F_{5/2}$ will transfer to high energy states of Tm^{3+} by non-radiative energy transmission. These electrons in the high energy states of Tm^{3+} can transfer to $^4T_1$ of Cr^{3+} in PLNPs and are caught by the electron traps. Similar to that just mentioned, after ceasing the

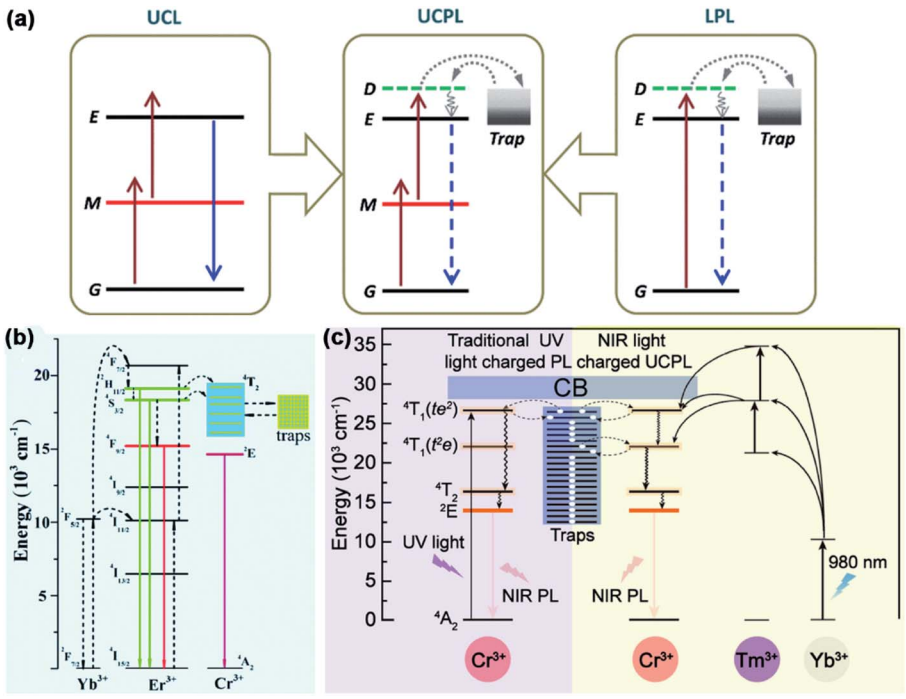

Fig. 7 (a) Schematic diagram of electronic structure engineering based on the anti-Stokes mechanism (adapted with permission from ref. 35. Copyright 2014 American Physical Society). (b) Scheme of electronic structure engineering by co-doping Yb^{3+}, Er^{3+}, and Cr^{3+} into ZGGO (adapted with permission from ref. 40. Copyright 2017 Royal Society of Chemistry). (c) Scheme of electronic structure engineering by constructing a composite structure with ZGGO:Cr^{3+} and β-$NaYbF_4$:Tm^{3+}@$NaYF_4$ (adapted with permission from ref. 104. Copyright 2017 American Chemical Society).

excitation, these electrons in the traps are slowly released to the energy levels of Cr^{3+} and turn back to $^4A_2$, generating persistent luminescence. In this way, effectively combining PLNPs with up-converted nanoparticles can also extend the excitation band to the NIR region.

Hence, the most effective way to construct NPLNPs is to dope up-conversion ions. The up-conversion effect allows the electrons to reach higher energy levels through NIR excitation and are captured by the electron traps. However, the current development of NPLNPs is still in its infancy, so there are still some problems with NPLNPs, including low quantum efficiency, and insufficient fluorescence intensity and lifetime after NIR excitation. These problems are the bottlenecks that may limit the further development of NPLNPs in the future.

4.2. Applications of NPLNPs in biomedicine

While studying how to construct NPLNPs, scientists have also paid attention to the application of NPNLPs in recent years, especially in biological imaging and imaging-guided therapy. In this section, we will introduce the latest applications of NPLNPs in biological imaging and imaging-guided therapy.

4.2.1. Bioimaging. Compared to UV and visible light, NIR exhibits deeper tissue penetration depth and lower tissue overheating. Benefiting from such advantages, NIR has been widely used as a light source for applications in deep-tissue imaging, playing important roles in understanding the biological mechanisms and disease diagnosis.[105,106] NPLNPs can be activated *via* 808 nm or 980 nm laser and emit visible light or NIR, and both of their excitation band and emission band are in the biological transparency window (600–1100 nm).[107,108] Therefore, NIR can effectively penetrate the deep tissue and activate NPLNPs *in vivo*. Besides, the emission from NPLNPs can also be detected *in vitro*.[109] Furthermore, NPLNPs can also be recharged *in vivo* several times, so they are suitable for long-term bioimaging and biological tracing in deep tissues.[40] In this regard, NPLNPs have received extensive interest by scientists as a substitute to traditional PLNPs for applications in long-term bioimaging and tracing.

In 2017, Feng and Li *et al.* assembled $NaYbF_4$:0.5% Tm^{3+}@$NaYF_4$ with ZGGO:Cr^{3+} in a two-phase system nanocluster.[104] $NaYbF_4$:0.5%Tm^{3+}@$NaYF_4$ can be effectively activated *via* 980 nm laser *in vivo* and generate the afterglow at 700 nm. Both the excitation and emission wavelengths are within the biologically transparent window, which means that using this nanocluster can effectively solve the problem of insufficient tissue penetration. According to the authors, these NPLNP nanoclusters can be activated in the lymphatic system and can be recharged several times *in vivo*. After stopping the excitation of the light source, the afterglow emission of NPLNPs can be detected only in the lymphatic vessels and there is no background fluorescence interference from other substrates. Therefore, the two-phase system nanoclusters have potential for being utilized in deep-tissue real-time lymphatic imaging in the future.

In addition, Zeng and Hao *et al.* also reported a NIR-to-NIR afterglow probe ZGGO:Yb^{3+},Er^{3+},Cr^{3+} for bioimaging.[40] This probe is rechargeable *in vivo* by a 980 nm laser and the excitation and emission bands are also both in the biologically transparent window. About 2 hours after the first excitation, the afterglow intensity is significantly reduced, which means that the electrons trapped in the traps are depleted. At this time, the 980 nm light source is used to excite the body again and the afterglow of this NPLNP can return to a higher intensity (Fig. 8). Therefore, the NPLNP probes can be activated in deep tissue and can also be recharged *in vivo*. Due to the features of deep penetration and recharging *in vivo*, it is available and promising for NPLNPs to be applied in renewable deep-tissue bioimaging.

In conclusion, compared to conventional bioimaging by fluorescent dyes or traditional PLNPs, NPLNPs exhibit advantages in bioimaging, such as low energy consumption, high tissue penetration, no autofluorescence, low tissue damage, and recharge *in vivo*. For these reasons, the application of NPLNPs in bioimaging will get more attention from researchers and versatile applications in bioimaging by NPLNPs can be envisaged in the future.

4.2.2. Guiding for disease treatment. Deep tissue tumours are also very common in clinical practice today. For the precise treatment of deep tissue tumours, NPLNPs can be repeatedly excited *in situ* by NIR in deep tissues, which solves the difficulty of traditional PLNPs, which cannot be excited in deep tissues. Therefore, NPLNPs can effectively serve as a light source for deep-tissue photodynamic therapy. Also, NPLNPs can effectively eliminate background fluorescence because of the long afterglow life, so they have great potential in guiding deep-tissue treatment.

Owing to the long persistent emission and NIR excitation, NPLNPs are advantageous as *in vivo* excitation sources for photodynamic therapy. Photodynamic therapy with NPLNPs can resolve the bottleneck of traditional photodynamic therapy. Hence, it is of great worth to develop NPLNPs for photodynamic therapy in the future. Recently, Zhang and Li *et al.* reported a unique rechargeable "optical battery" implant for long-term photodynamic therapy, which can be recharged *in vivo* by a 980 nm NIR laser and can persistently emit for about 30 min after ceasing charging.[98] This optical battery was assembled by embedding green persistent luminescence materials, up-conversion phosphors, and photosensitizers into biocompatible polydimethylsiloxane (PDMS). As demonstrated by the authors, the optical battery exhibits excellent bio-stability and flexibility, and yields ROS efficiently without photothermal effect (Fig. 9). Aimed at different nidus sites, the shape and size of the battery can also be easily controlled. Moreover, the optical battery can be excited in the deep tissue up to 4 mm and can yield singlet oxygen persistently. This means the optical battery can be utilized in deep-tissue photodynamic therapy and the drawbacks of traditional photodynamic therapy such as low tissue penetration and insufficient ROS can be overcome. The results *in vitro* and *in vivo* indicate that this optical battery can effectively inhibit tumour proliferation, even hypoxic tumour proliferation. Nevertheless, even if NPLNPs show great advantages in photodynamic therapy, the research on photodynamic therapy based on NPLNPs is still in the initial stage and more efficient strategies must be presented.

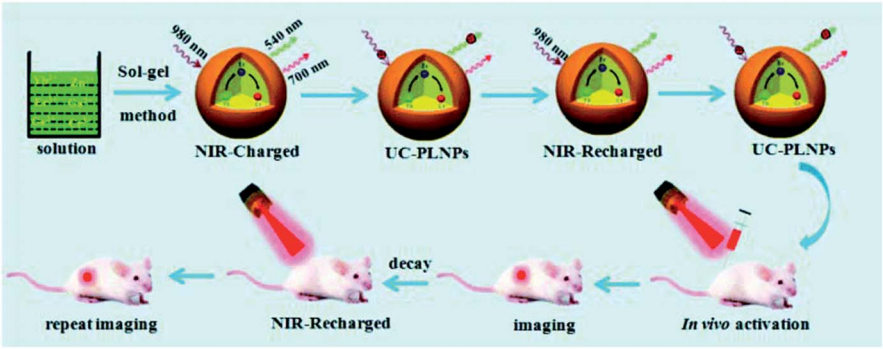

Fig. 8 Schematic diagram of long-term bioimaging of deep tissue with reproducible NPLNPs (adapted with permission from ref. 40. Copyright 2017 Royal Society of Chemistry).

In addition, with the feasibility of long-term bioimaging, imaging-guided therapy has also received much more interest. Macrophage-based immunotherapy is one of the most important strategies of tumour targeted therapy. The macrophages can enter the tumour micro-environment and restrain the growth of the tumour by phagocytosis and cytokine secretion. However, traditional macrophage-based immunotherapy cannot be effectively tracked *in vivo* without activation *in situ*.[110–112] Recently, Wang and Chang *et al.* developed Zn_2SiO_4:Mn^{2+},Y^{3+},Yb^{3+},Tm^{3+} NPLNPs for imaging-guided cell therapy *in vivo*.[113] By labelling tumour associated macrophages by Zn_2SiO_4:Mn^{2+},Y^{3+},Yb^{3+},Tm^{3+}, the limitation of traditional macrophage-based immunotherapy can be overcome. According to the authors, the NPLNPs can be endocytosed by the macrophages and exhibit good biocompatibility in the macrophages. With the feature that Zn_2SiO_4:Mn^{2+},Y^{3+},Yb^{3+},Tm^{3+} can be excited *in vivo* by NIR, this NPLNP can be effectively utilized to detect the distribution and location of macrophages in cell therapy (Fig. 10). In this condition, it can solve the limitation that traditional cell therapy cannot be visually traced during the therapy processes.

Except for that mentioned before, tracking drug carriers is also one of the important strategies for accurate treatment. However, imaging and tracking the distribution of drug carriers in deep tissue is still a challenging topic. NPLNPs can be effectively stimulated by NIR in deep tissues, making them great candidates for tracking drug carriers in deep tissues. In 2018, Zhang *et al.* reported a unique multifunctional nano platform for multimodal imaging and cancer treatment.[114] They conjugated NPLNP ($Gd_3Ga_5O_{12}$:Cr^{3+},Nd^{3+}) together with mesoporous silica and realized the integration of imaging and drug loading. This NPLNP can be excited at 808 nm and generates afterglow at 1067 nm. Due to lower photon scattering and deeper penetration, it has proven to be more suitable for deep-tissue imaging with high signal-to-noise ratio. In addition, the platform can be used not only for fluorescence imaging to track the drug carriers but also for magnetic resonance imaging to track the drug carriers. This means that it has the advantages of multimodal imaging. Therefore, we can expect the platform to have better applications in future precision treatment.

In summary, due to the good tissue penetrability of NIR, NPLNPs have great potential as probes for deep tissue imaging to guide precise treatment. For these reasons, researchers should pay more attention to the application of NPLNPs in the construction of precision treatment platforms and the

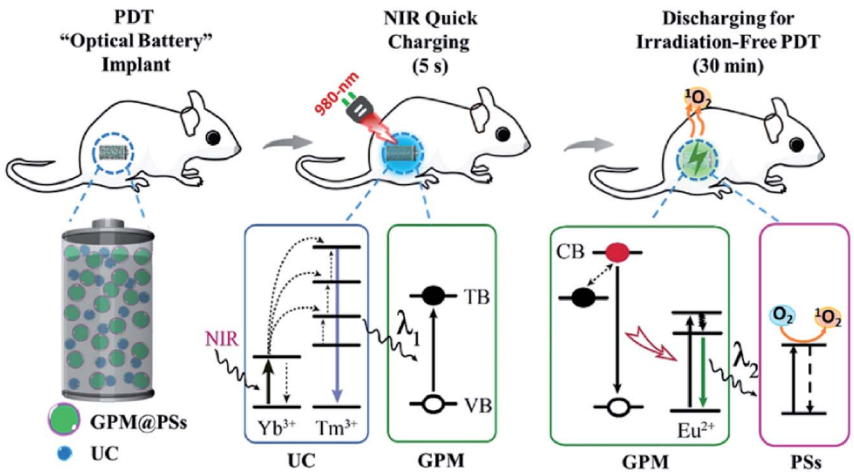

Fig. 9 Schematic diagram showing the use of rechargeable NPLNPs for constructing "optical battery" implants for radiation-free photodynamic therapy (adapted with permission from ref. 98. Copyright 2018 Elsevier).

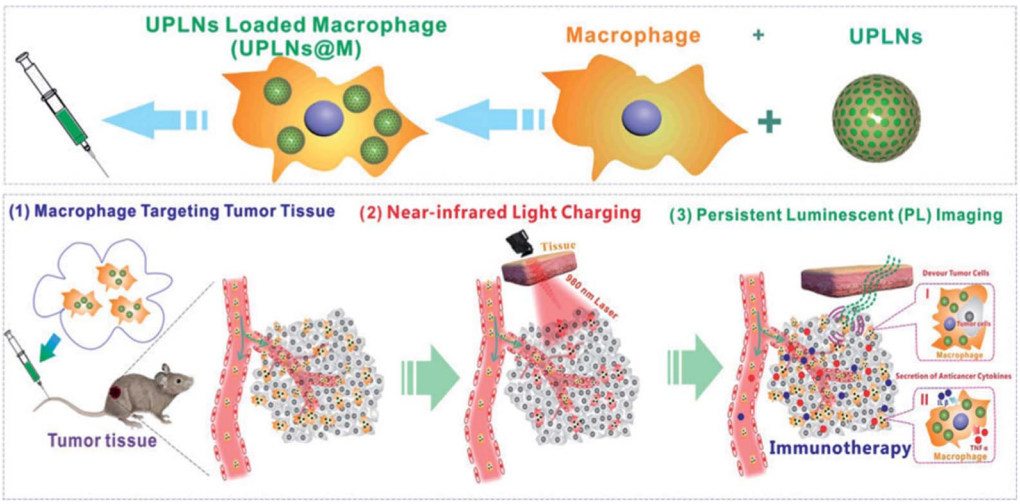

Fig. 10 Schematic diagram of bioimaging guide for immunotherapy tracking macrophages with NPLNPs (adapted with permission from ref. 113. Copyright 2018 American Chemical Society).

widespread application of NPLNPs in deep tissue therapy in the future can be imagined.

5. Conclusion and outlook

PLNPs, a series of novel luminescent materials with long decay time, have received major interest in biological science. Compared to PLNPs excited by UV, VPLNPs and NPLNPs have the excitation band in the visible light region and the NIR region, displaying several advantages such as low tissue damage, deep tissue penetration, and high signal-to-noise ratio, receiving intensive interest in recent years. In this review, we have introduced electronic structure engineering strategy for constructing VPLNPs based on Stokes mechanism and constructing NPLNPs based on anti-Stokes mechanism. Besides, we have also summarized their applications in biodetection, bioimaging, and guidance for treatment. Despite some progress that has been made, the development of VPLNPs and NPLNPs also faces several bottlenecks. The quantum efficiency of VPLNPs and NPLNPs needs to be enhanced, and new construction strategies are still in great demand. Also, it remains difficult to precisely control the luminescent properties of VPLNPs and NPLNPs, including their emission wavelength, emission intensity, and afterglow duration. Hence, one of the most important directions for reforming VPLNPs and NPLNPs is to improve the quantum efficiency and to develop more controllable synthetic strategies in the future. In order to achieve these targets, more progress must be made in the technology of electronic structure engineering. For example, developing more synthetic control methods can effectively promote the development of synthetic strategies for VPLNPs and NPLNPs, such as doping strategies and etching technologies. Furthermore, the development of theoretical calculation can also be helpful in guiding the design of more unique VPLNPs and NPLNPs, especially spin-orbital coupling and relativistic effect for rare earth ions, which can improve the calculation accuracy of the spectrum. With the improvement in synthesis and properties of VPLNPs and NPLNPs, they will have more comprehensive applications in various fields and promote the development of not only biomedical research but also many other fields.

Conflicts of interest

There are no conflicts to declare.

Acknowledgements

This work was supported by the National Key R&D Program of China (2017YFA0208000), the National Natural Science Foundation of China (21925401, 21904100, 21675120), and the National Postdoctoral Program for Innovative Talents (BX20180223).

References

1 A. Tuerdi and A. Abdukayum, *RSC Adv.*, 2019, **9**, 17653–17657.
2 Y. Wang, Z. Li, Q. Lin, Y. Wei, J. Wang, Y. Li, R. Yang and Q. Yuan, *ACS Sens.*, 2019, **4**, 2124–2130.
3 A. Bessière, S. K. Sharma, N. Basavaraju, K. R. Priolkar, L. Binet, B. Viana, A. J. J. Bos, T. Maldiney, C. Richard, D. Scherman and D. Gourier, *Chem. Mater.*, 2014, **26**, 1365–1373.
4 P. J. Liu and Y. L. Liu, *Chin. Chem. Lett.*, 2000, **11**, 843–846.
5 Z. Zhou, W. Zheng, J. Kong, Y. Liu, P. Huang, S. Zhou, Z. Chen, J. Shi and X. Chen, *Nanoscale*, 2017, **9**, 6846–6853.
6 H. Liu, X. Hu, J. Wang, M. Liu, W. Wei and Q. Yuan, *Chin. Chem. Lett.*, 2018, **29**, 1641–1644.
7 R. Shrivastava and J. Kaur, *Chin. Chem. Lett.*, 2015, **26**, 1187–1190.

8 Y. Xia, X. Huang, W. Wu, W. Li, Z. Li and G. Han, *J. Lumin.*, 2019, **207**, 53–57.
9 N. Yu, Y. Li, Z. Li and G. Han, *Sci. China: Chem.*, 2018, **61**, 757–758.
10 P. F. Smet, D. Poelman and M. P. Hehlen, *Opt. Mater. Express*, 2012, **2**, 452–454.
11 F. Liu, W. Yan, Y. J. Chuang, Z. Zhen, J. Xie and Z. Pan, *Sci. Rep.*, 2013, **3**, 1554.
12 Z. Pan, Y. Y. Lu and F. Liu, *Nat. Mater.*, 2011, **11**, 58.
13 T. Jüstel, H. Nikol and C. Ronda, *Angew. Chem., Int. Ed.*, 1998, **37**, 3084–3103.
14 Z. H. Li, Q. Wang, Y. Q. Wang, Q. Q. Ma, J. Wang, Z. H. Li, Y. X. Li, X. B. Lv, W. Wei, L. Chen and Q. Yuan, *Nano Res.*, 2018, **11**, 6167–6176.
15 J. Tang, Y. Su, D. Deng, L. Zhang, N. Yang and Y. Lv, *Analyst*, 2016, **141**, 5366–5373.
16 J. Wang, Q. Ma, H. Liu, Y. Wang, H. Shen, X. Hu, C. Ma, Q. Yuan and W. Tan, *Anal. Chem.*, 2017, **89**, 12764–12770.
17 L. Song, X. H. Lin, X. R. Song, S. Chen, X. F. Chen, J. Li and H.-H. Yang, *Nanoscale*, 2017, **9**, 2718–2722.
18 J. L. Li, J. P. Shi, C. C. Wang, P. H. Li, Z. F. Yu and H. W. Zhang, *Nanoscale*, 2017, **9**, 8631–8638.
19 Y. C. Lu, C. X. Yang and X. P. Yan, *Nanoscale*, 2015, **7**, 17929–17937.
20 J. Shi, X. Sun, J. Zhu, J. Li and H. Zhang, *Nanoscale*, 2016, **8**, 9798–9804.
21 Y. Jiang, J. Huang, X. Zhen, Z. Zeng, J. Li, C. Xie, Q. Miao, J. Chen, P. Chen and K. Pu, *Nat. Commun.*, 2019, **10**, 2064.
22 E. Teston, T. Maldiney, I. Marangon, J. Volatron, Y. Lalatonne, L. Motte, C. Boisson-Vidal, G. Autret, O. Clement, D. Scherman, F. Gazeau and C. Richard, *Small*, 2018, **14**, e1800020.
23 E. M. Rodríguez, G. López-Peña, E. Montes, G. Lifante, J. G. Solé, D. Jaque, L. A. Diaz-Torres and P. Salas, *Appl. Phys. Lett.*, 2017, **111**, 081901.
24 J. Wang, Q. Ma, W. Zheng, H. Liu, C. Yin, F. Wang, X. Chen, Q. Yuan and W. Tan, *ACS Nano*, 2017, **11**, 8185–8191.
25 B. Qu, B. Zhang, L. Wang, R. Zhou and X. C. Zeng, *Chem. Mater.*, 2015, **27**, 2195–2202.
26 F. Wang, B. Yang, D. Liu, W. Ma, X. Chen and Y. Dai, *Spectrochim. Acta, Part A*, 2014, **126**, 46–52.
27 H. Chen, X. Sun, G. D. Wang, K. Nagata, Z. Hao, A. Wang, Z. Li, J. Xie and B. Shen, *Mater. Horiz.*, 2017, **4**, 1092–1101.
28 Z. Li, L. Huang, Y. Zhang, Y. Zhao, H. Yang and G. Han, *Nano Res.*, 2017, **10**, 1840–1846.
29 Y. Li, M. Gecevicius and J. Qiu, *Chem. Soc. Rev.*, 2016, **45**, 2090–2136.
30 Y. Xia, H. Ou, W. Li, G. Han and Z. Li, *Nanomaterials*, 2018, **8**, 260.
31 T. Sun, J. Wang, X. Chi, Y. Lin, Z. Chen, X. Ling, C. Qiu, Y. Xu, L. Song, W. Chen and C. Su, *ACS Catal.*, 2018, **8**, 7585–7592.
32 Y. Chen, S. Huang, X. Ji, K. Adepalli, K. Yin, X. Ling, X. Wang, J. Xue, M. Dresselhaus, J. Kong and B. Yildiz, *ACS Nano*, 2018, **12**, 2569–2579.
33 C. Forsythe, X. Zhou, K. Watanabe, T. Taniguchi, A. Pasupathy, P. Moon, M. Koshino, P. Kim and C. R. Dean, *Nat. Nanotechnol.*, 2018, **13**, 566–571.
34 M. Schwarze, W. Tress, B. Beyer, F. Gao, R. Scholz, C. Poelking, K. Ortstein, A. A. Günther, D. Kasemann, D. Andrienko and K. Leo, *Science*, 2016, **352**, 1446.
35 F. Liu, Y. Liang and Z. Pan, *Phys. Rev. Lett.*, 2014, **113**, 177401.
36 Z. Li, Y. Zhang, X. Wu, X. Wu, R. Maudgal, H. Zhang and G. Han, *Adv. Sci.*, 2015, **2**, 1500001.
37 T. Maldiney, A. Bessière, J. Seguin, E. Teston, S. K. Sharma, B. Viana, A. J. J. Bos, P. Dorenbos, M. Bessodes, D. Gourier, D. Scherman and C. Richard, *Nat. Mater.*, 2014, **13**, 418.
38 X. Sun, J. Shi, S. Zheng, J. Li, S. Wang and H. Zhang, *J. Lumin.*, 2018, **204**, 520–527.
39 J. Wang, Q. Ma, X. X. Hu, H. Liu, W. Zheng, X. Chen, Q. Yuan and W. Tan, *ACS Nano*, 2017, **11**, 8010–8017.
40 Z. Xue, X. Li, Y. Li, M. Jiang, G. Ren, H. Liu, S. Zeng and J. Hao, *Nanoscale*, 2017, **9**, 7276–7283.
41 Q. Lin, Z. Li and Q. Yuan, *Chin. Chem. Lett.*, 2019, **30**, 1547–1556.
42 J. Wang, Q. Ma, Y. Wang, H. Shen and Q. Yuan, *Nanoscale*, 2017, **9**, 6204–6218.
43 X. Ni, X. Zhang, X. Duan, H. L. Zheng, X. S. Xue and D. Ding, *Nano Lett.*, 2019, **19**, 318–330.
44 X. Zhou, G. Ju, T. Dai, Y. Li, H. Wu, Y. Jin and Y. Hu, *Chem.–Asian J.*, 2019, **14**, 1506–1514.
45 W. Jiang, L. Huang, F. Mo, Y. Zhong, L. Xu and F. Fu, *J. Mater. Chem. B*, 2019, **7**, 3019–3026.
46 J. Shi, X. Sun, J. Li, H. Man, J. Shen, Y. Yu and H. Zhang, *Biomaterials*, 2015, **37**, 260–270.
47 F. Yang, M. Wilkinson, E. J. Austin and K. P. O'Donnell, *Phys. Rev. Lett.*, 1993, **70**, 323–326.
48 X. Peng, F. Song, E. Lu, Y. Wang, W. Zhou, J. Fan and Y. Gao, *J. Am. Chem. Soc.*, 2005, **127**, 4170–4171.
49 R. W. Martin, P. G. Middleton, K. P. O'Donnell and W. Van der Stricht, *Appl. Phys. Lett.*, 1999, **74**, 263–265.
50 Z. Zhou, W. Zheng, J. Kong, Y. Liu, P. Huang, S. Zhou, Z. Chen, J. Shi and X. Chen, *Nanoscale*, 2017, **9**, 6846–6853.
51 R. Chen, *J. Electrochem. Soc.*, 1969, **116**, 1254–1257.
52 J. Ueda, J. L. Leaño, C. Richard, K. Asami, S. Tanabe and R.-S. Liu, *J. Mater. Chem. C*, 2019, **7**, 1705–1712.
53 Y. Du, Y. Jiang, T. Sun, J. Zhao, B. Huang, D. Peng and F. Wang, *Adv. Mater.*, 2018, **31**, e1807062.
54 Z. Yu, B. Liu, W. Pan, T. Zhang, L. Tong, N. Li and B. Tang, *Chem. Commun.*, 2018, **54**, 3504–3507.
55 W. Zheng, P. Huang, D. Tu, E. Ma, H. Zhu and X. Chen, *Chem. Soc. Rev.*, 2015, **44**, 1379–1415.
56 Y. Lu, M. Zhu, W. Li, B. Lin, X. Dong, Y. Chen, X. Xie, J. Guo and M. Li, *J. Cell. Mol. Med.*, 2016, **20**, 549–558.
57 J. D. Cohen, A. A. Javed, C. Thoburn, F. Wong, J. Tie, P. Gibbs, C. M. Schmidt, M. T. Yip-Schneider, P. J. Allen, M. Schattner, R. E. Brand, A. D. Singhi, G. M. Petersen, S. M. Hong, S. C. Kim, M. Falconi, C. Doglioni, M. J. Weiss, N. Ahuja, J. He, M. A. Makary, A. Maitra, S. M. Hanash, M. Dal Molin, Y. Wang, L. Li, J. Ptak, L. Dobbyn, J. Schaefer, N. Silliman, M. Popoli, M. G. Goggins, R. H. Hruban, C. L. Wolfgang, A. P. Klein, C. Tomasetti, N. Papadopoulos, K. W. Kinzler,

B. Vogelstein and A. M. Lennon, *Proc. Natl. Acad. Sci. U. S. A.*, 2017, **114**, 10202–10207.
58 J. D. Lapek Jr, P. Greninger, R. Morris, A. Amzallag, I. Pruteanu-Malinici, C. H. Benes and W. Haas, *Nat. Biotechnol.*, 2017, **35**, 983.
59 W. Pan, B. Liu, X. Gao, Z. Yu, X. Liu, N. Li and B. Tang, *Nanoscale*, 2018, **10**, 14264–14271.
60 N. Li, W. Diao, Y. Han, W. Pan, T. Zhang and B. Tang, *Chem.–Eur. J.*, 2014, **20**, 16488–16491.
61 N. Li, Y. Li, Y. Han, W. Pan, T. Zhang and B. Tang, *Anal. Chem.*, 2014, **86**, 3924–3930.
62 J. Yang, Y. Liu, Y. Zhao, Z. Gong, M. Zhang, D. Yan, H. Zhu, C. Liu, C. Xu and H. Zhang, *Chem. Mater.*, 2017, **29**, 8119–8131.
63 A. S. Paterson, B. Raja, G. Garvey, A. Kolhatkar, A. E. Hagstrom, K. Kourentzi, T. R. Lee and R. C. Willson, *Anal. Chem.*, 2014, **86**, 9481–9488.
64 J. M. Liu, X. Y. Yuan, H. L. Liu, D. Cheng and S. Wang, *RSC Adv.*, 2018, **8**, 28414–28420.
65 M. Wang, M. Li, A. Yu, J. Wu and C. Mao, *ACS Appl. Mater. Interfaces*, 2015, **7**, 28110–28115.
66 M. Wang, M. Li, A. Yu, Y. Zhu, M. Yang and C. Mao, *Adv. Funct. Mater.*, 2017, **27**, 1606243.
67 H. Liu, Y. Sun, Z. Li, J. Yang, A. A. Aryee, L. Qu, D. Du and Y. Lin, *Nanoscale*, 2019, **11**, 8458–8463.
68 J. Wang, T. Wei, X. Li, B. Zhang, J. Wang, C. Huang and Q. Yuan, *Angew. Chem., Int. Ed.*, 2014, **53**, 1616–1620.
69 J. M. Baumes, J. J. Gassensmith, J. Giblin, J.-J. Lee, A. G. White, W. J. Culligan, W. M. Leevy, M. Kuno and B. D. Smith, *Nat. Chem.*, 2010, **2**, 1025–1030.
70 S. C. Lee, H. H. Park, S. H. Kim, S. H. Koh, S. H. Han and M. Y. Yoon, *Anal. Chem.*, 2019, **91**, 5573–5581.
71 J. Chen, H. Qiu, M. Zhang, T. Gu, S. Shao, Y. Huang and S. Zhao, *Biosens. Bioelectron.*, 2015, **68**, 550–555.
72 P. Zou, Y. Liu, H. Wang, J. Wu, F. Zhu and H. Wu, *Biosens. Bioelectron.*, 2016, **79**, 29–33.
73 F. Qu, Y. Liu, R. Kong and J. You, *Microchim. Acta*, 2017, **184**, 4417–4424.
74 M. Hoang, P. J. J. Huang and J. Liu, *ACS Sens.*, 2016, **1**, 137–143.
75 X. Wang, B. Liu and J. Liu, *Langmuir*, 2018, **34**, 15871–15877.
76 D. Tian, X. J. Liu, R. Feng, J. L. Xu, J. Xu, R. Y. Chen, L. Huang and X. H. Bu, *ACS Appl. Mater. Interfaces*, 2018, **10**, 5618–5625.
77 J. Chen, Q. Chen, C. Gao, M. Zhang, B. Qin and H. Qiu, *J. Mater. Chem. B*, 2015, **3**, 964–967.
78 Y. Han, C. Ding, J. Zhou and Y. Tian, *Anal. Chem.*, 2015, **87**, 5333–5339.
79 H. Huang, F. Dong and Y. Tian, *Anal. Chem.*, 2016, **88**, 12294–12302.
80 W. Fan, N. Lu, C. Xu, Y. Liu, J. Lin, S. Wang, Z. Shen, Z. Yang, J. Qu, T. Wang, S. Chen, P. Huang and X. Chen, *ACS Nano*, 2017, **11**, 5864–5872.
81 X. Qian and Z. Xu, *Chem. Soc. Rev.*, 2015, **44**, 4487–4493.
82 Q. Zhao, C. Huang and F. Li, *Chem. Soc. Rev.*, 2011, **40**, 2508–2524.
83 Q. Zhao, M. Yu, L. Shi, S. Liu, C. Li, M. Shi, Z. Zhou, C. Huang and F. Li, *Organometallics*, 2010, **29**, 1085–1091.
84 H. Wang, J. Chang, M. Shi, W. Pan, N. Li and B. Tang, *Angew. Chem., Int. Ed.*, 2019, **58**, 1057–1061.
85 N. Yu, L. Huang, Y. Zhou, T. Xue, Z. Chen and G. Han, *Adv. Healthcare Mater.*, 2019, **8**, e1801132.
86 D. D. Zhang, J. M. Liu, N. Song, Y. Y. Liu, M. Dang, G. Z. Fang and S. Wang, *J. Mater. Chem. B*, 2018, **6**, 1479–1488.
87 J. M. Liu, D. D. Zhang, G. Z. Fang and S. Wang, *Biomaterials*, 2018, **165**, 39–47.
88 L. J. Chen, S. K. Sun, Y. Wang, C. X. Yang, S. Q. Wu and X. P. Yan, *ACS Appl. Mater. Interfaces*, 2016, **8**, 32667–32674.
89 H. Chen, B. Zheng, C. Liang, L. Zhao, Y. Zhang, H. Pan, W. Ji, X. Gong, H. Wang and J. Chang, *Mater. Sci. Eng. C*, 2017, **79**, 372–381.
90 T. Maldiney, B. Ballet, M. Bessodes, D. Scherman and C. Richard, *Nanoscale*, 2014, **6**, 13970–13976.
91 L. J. Chen, C. X. Yang and X. P. Yan, *Anal. Chem.*, 2017, **89**, 6936–6939.
92 M. Luan, J. Chang, W. Pan, Y. Chen, N. Li and B. Tang, *Anal. Chem.*, 2018, **90**, 10951–10957.
93 H. D. Cui, D. H. Hu, J. N. Zhang, G. H. Gao, C. F. Zheng, P. Gong, X. H. Xi, Z. H. Sheng and L. T. Cai, *Chin. Chem. Lett.*, 2017, **28**, 1391–1398.
94 L. L. Rui, H. L. Cao, Y. D. Xue, L. C. Liu, L. Xu, Y. Gao and W. A. Zhang, *Chin. Chem. Lett.*, 2016, **27**, 1412–1420.
95 L. Song, P. P. Li, W. Yang, X. H. Lin, H. Liang, X. F. Chen, G. Liu, J. Li and H. H. Yang, *Adv. Funct. Mater.*, 2018, **28**, 1707496.
96 Z. Yu, P. Zhou, W. Pan, N. Li and B. Tang, *Nat. Commun.*, 2018, **9**, 5044.
97 Y. Zhu, W. Lin, W. Zhang, Y. Feng, Z. Wu, L. Chen and Z. Xie, *Chin. Chem. Lett.*, 2017, **28**, 1875–1877.
98 L. Hu, P. Wang, M. Zhao, L. Liu, L. Zhou, B. Li, F. H. Albaqami, A. M. El-Toni, X. Li, Y. Xie, X. Sun and F. Zhang, *Biomaterials*, 2018, **163**, 154–162.
99 R. Abdurahman, C. X. Yang and X. P. Yan, *Chem. Commun.*, 2016, **52**, 13303–13306.
100 Q. Chen, Y. Ma, J. Zhao, M. Zhao, W. Li, Q. Liu, L. Xiong, W. Wu and Z. Hong, *Chin. Chem. Lett.*, 2018, **29**, 1171–1178.
101 T. Ai, W. Shang, H. Yan, C. Zeng, K. Wang, Y. Gao, T. Guan, C. Fang and J. Tian, *Biomaterials*, 2018, **167**, 216–225.
102 L. Huang, Y. Zhao, H. Zhang, K. Huang, J. Yang and G. Han, *Angew. Chem., Int. Ed.*, 2017, **56**, 14400–14404.
103 F. Auzel, *Chem. Rev.*, 2004, **104**, 139–174.
104 X. Qiu, X. Zhu, M. Xu, W. Yuan, W. Feng and F. Li, *ACS Appl. Mater. Interfaces*, 2017, **9**, 32583–32590.
105 R. Zou, J. Huang, J. Shi, L. Huang, X. Zhang, K. L. Wong, H. Zhang, D. Jin, J. Wang and Q. Su, *Nano Res.*, 2017, **10**, 2070–2082.
106 Y. Li, S. Zhou, Y. Li, K. Sharafudeen, Z. Ma, G. Dong, M. Peng and J. Qiu, *J. Mater. Chem. C*, 2014, **2**, 2657–2663.
107 G. Hong, A. L. Antaris and H. Dai, *Nat. Biomed. Eng.*, 2017, **1**, 0010.
108 A. M. Smith, M. C. Mancini and S. Nie, *Nat. Nanotechnol.*, 2009, **4**, 710–711.

109 K. Y. Zhang, Q. Yu, H. Wei, S. Liu, Q. Zhao and W. Huang, *Chem. Rev.*, 2018, **118**, 1770–1839.
110 S. Zanganeh, R. Spitler, G. Hutter, J. Q. Ho, M. Pauliah and M. Mahmoudi, *Immunotherapy*, 2017, **9**, 819–835.
111 A. Weigert, D. Sekar and B. Brüne, *Immunotherapy*, 2008, **1**, 83–95.
112 Z. Huang, Z. Zhang, Y. Jiang, D. Zhang, J. Chen, L. Dong and J. Zhang, *J. Controlled Release*, 2012, **158**, 286–292.
113 B. Zheng, Y. Bai, H. Chen, H. Pan, W. Ji, X. Gong, X. Wu, H. Wang and J. Chang, *ACS Appl. Mater. Interfaces*, 2018, **10**, 19514–19522.
114 J. Shi, X. Sun, S. Zheng, J. Li, X. Fu and H. Zhang, *Biomaterials*, 2018, **152**, 15–23.